analytical chemistry

pubs.acs.org/ac Article

Internal Calibration without Internal Calibrants by Mass Difference Analysis in FT-ICR Mass Spectrometry

Ryan P. Rodgers,* Christopher L. Hendrickson, Christopher A. Holder Montenegro, Alvaro J. Tello-Rodriguez, Teja Potu, Benjohn Shung, Mason Hagan, Chad R. Weisbrod, Pierre Giusti, Christopher P. Rüger, Martha L. Aguilera, and Germain Salvato Vallverdu*

Cite This: *Anal. Chem.* 2025, 97, 18543−18552 Read Online

ACCESS | Metrics & More | Article Recommendations | Supporting Information

ABSTRACT: We report an improved, fully automated method of mass spectral calibration that relies on mass differences instead of internal calibrants. First, we introduce the mass difference spectrum and note that confident elemental formulas can be assigned to the most abundant mass differences between 0 and 50 Daltons, even for poorly calibrated data. Second, we demonstrate recalibration to as low as 80 ppb rms error by optimizing the measured mass differences, without reference to any known masses in the spectrum. Finally, the improved global calibration facilitates a subsequent "walking" calibration that proceeds through simple matrix intersection calculations and ultimately yields confident molecular formula assignments. We apply the method to a variety of complex samples, including petroleum, dissolved organic matter (natural, pyrogenic, anthropogenic), biomass, biofuels, lithium-ion batteries, polymers, aerosols, and emerging environmental contaminants, and others that contain repeated series of mass differences (characteristic "building blocks"). Obvious for polymers, but less so for other sample types, the repeated mass spacings can arise from thermal/chemical degradation pathways, combustion/pyrolysis, molecular synthesis methodologies, and/or electrochemical reactions, which are exploited herein for mass spectral recalibration. The method is implemented in an open-source, Python-based, software platform, PyC2MC, which also enables automated batch file processing of time-resolved, complex mass spectral data.

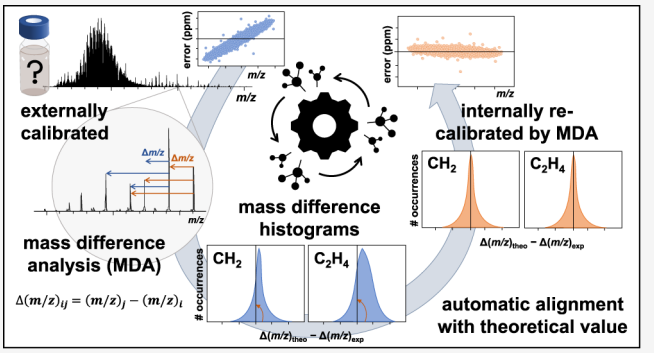

Fourier transform ion cyclotron resonance (FT-ICR) mass spectrometry facilitates research in a diverse array of complex mixture applications, including nonterrestrial organics,[1−5] degradation products from the built environment,[6−14] natural organic matter,[15−23] emerging contaminants,[22,24−29] petroleum,[30−35] photooxidation products,[19,20,36−40] biofuels,[7,41−46] organic leachates,[21,41,45,47,48] and organic aerosols.[49−54] These challenging samples are often rich in heteroatoms (e.g., S, N, O, F, Cl, Br, Na, B, Fe, Ni, V, Si) and frequently lack homologous series that span a large portion of the molecular weight distribution (for internal recalibration), which poses a significant data processing challenge. Furthermore, continuous instrumental advances[55−60] have facilitated faster data acquisition speed, higher resolving power, and increased mass accuracy. Combined, these factors have expanded the number of LC-FT-ICR MS applications, and with the recent installation of the 18 T TIMS FT-ICR MS (iC2MC, Rouen, France),[61] have resulted in data calibration and elemental composition assignment as the primary issues that slow sample throughput.

In the past, strategies to overcome these challenges have exploited "building blocks" (repeated mass spectral spacings),[62−64] isotopic depletion[65,66] or enrichment,[67] isotopic "fine structure",[68−70] chemical bonding rules, H/C and other elemental ratios (as constrained by databases), as well as knowledge about the sample type and ionization modes employed, to arrive at the most likely (and chemically correct) molecular formula. Largely summarized in the work of Kind and Fiehn,[71] these "golden rules" have been used collectively (or in part) to confidently assign molecular formulas in complex matrices for decades. In such workflows, a homologous series (e.g., CH_2) of an identified elemental composition is often used for subsequent internal calibration. Initially reported in 1963 by Edward Kendrick,[72] the exploitation of repeated mass spacings in petroleum mass spectra was used to reduce the size of "tables of precise masses" to a manageable number of entries. Building on the work of

Received: April 22, 2025
Revised: July 24, 2025
Accepted: August 7, 2025
Published: August 19, 2025

Beynon,[73] his modified version of these tables normalized the mass of a CH_2 unit to exactly 14, thereby imparting the same mass defect (later to be known as the Kendrick mass defect (KMD)) for all members of a homologous series. The approach has been exploited in many areas of research outside the original field of Petroleomics.[28,64,74−79]

Recently, the concept of utilizing mass differences to address various data processing challenges has been demonstrated. In 2006, Kujawinski and Behn introduced an automated Compound Identification Algorithm (CIA) for accurate determination of the molecular formulas in complex organic mixtures analyzed by FT-ICR MS through "formula extension."[62] Perminova et al. expanded this idea with the total mass difference statistics algorithm, to again address complex dissolved organic matter mass spectra, but extended it to larger mass (>50 Da) "building blocks" through the concept of "virtual elements."[63] Schmitt-Kopplin then updated Kendrick's approach to identify boron-containing complexes in DOM through the mass difference between ^{11}B and ^{10}B.[23] Notably, the authors demonstrated the accuracy of small mass differences (albeit for internally calibrated mass spectra) through an allowable match error of ± 110 μDa. Primarily focused on confident molecular formula assignment, these and other reports have introduced the concept of exploiting the interconnectivity of peaks within a complex mixture to simplify data processing (in these cases, elemental composition assignment), similar to Kendrick's approach more than 50 years ago.[80−85]

Known mass spacings in mass spectra can also be utilized for recalibration. Bruce et al. introduced DeCal (Deconvolution of Coulombic affected linearity) in 1999, to correct space-charge induced mass shifts in ICR without the need for internal calibrants.[86] In 2005, Wu et al. introduced COFI (Calibration Optimization on Fragment Ions),[87] a method for spectral recalibration in tandem MS applications that was designed to correct space-charge effects that utilized graph theory techniques developed by Xu et al.[82] Amster and Jing later built on the idea to demonstrate space-charge corrected recalibration for MALDI FT-ICR mass spectra, where shot-to-shot variations in ion abundance inevitably led to abnormally large mass errors.[88] Gavard et al. continued the evolution to GC FT-ICR MS applications to account for scan-to-scan space charge differences[89] and in the same year, Castilla et al. demonstrated a correction in direct inlet probe MS for lignocellulosic biomass analysis.[90] Despite success, the use of mass differences in ICR has been limited to space-charge correction (addition of a C term to the calibration equation) of the externally determined calibration coefficients (A & B), which yields mass errors in the ppm range. To date, the "gold standard" in the recalibration of complex FT-ICR mass spectra remains the "walking" internal calibration method[55] introduced by Savory et al. in 2011, which minimizes systematic errors by breaking the mass spectrum into multiple, consecutive m/z segments, each with their own calibration coefficients (A, B, and C (if desired)).[91]

Herein, we use mass difference analysis (MDA) for global calibration, walking calibration, and elemental composition assignment to enable automated processing of FT-ICR MS data. Mass difference spectra are calculated to identify the elemental and isotopic compositions of abundant mass repeat units, which enables calibration across diverse sample types. We evaluate the accuracy of small (<50 Da) mass differences in mass spectra. Unique, assigned mass differences (e.g., H_2, CH_2, C, or O) are then used to recalibrate the entire mass spectrum by optimization of the A and B calibration coefficients, in the Ledford equation,[92] for each mass difference pair so that the measured $\Delta m/z$ minus the theoretical $\Delta m/z$ is minimized. This enables accurate recalibration of the mass spectrum (~80 ppb rms error, as determined after elemental composition assignment) without internal calibrants through optimum selection of a single set of optimized A and B coefficients. Once recalibrated, known mass difference networks that span the entire mass range facilitate elemental composition assignment of a network that is subsequently used for internal "walking" calibration.[91] The method eliminates the need for internal standards and extends the capability of FT-ICR MS to confidently and exhaustively assign molecular formulas to increasingly complex mixtures through confident calibration. Further, the method incorporates quantized mass differences rooted in the precise masses of elemental particles, which takes advantage of forbidden regions in the mass difference space, where certain elemental combinations are absent due to the constraints of the periodic table.[93]

EXPERIMENTAL

Samples. Two representative complex mixtures were employed for the study. Middle Eastern heavy vacuum gas oil (HVGO) was used as received. A commercially available biomass pyrolyzate (BO), generated from fast pyrolysis of pinewood, was provided by BTG BTL (Enschede, Netherlands) company to TotalEnergies Research & Technology Gonfreville (Harfleur, France). The HVGO sample was first diluted in toluene to a concentration of 10 mg/mL and further diluted to a final concentration of 100 μg/mL (APPI). A bio-oil stock solution, 10 mg/mL in 1:1 (vol) toluene:methanol, was diluted in methanol to a final concentration of 50 μg/mL for mass spectral analysis (ESI).

FT-ICR Mass Spectral Analysis. Negative-ion electrospray ionization (−ESI) and positive-ion atmospheric pressure photoionization (+APPI) were employed for the analyses. For -ESI, ionization was facilitated using a needle voltage of −3.2 kV and a sample flow rate of 0.5 μL/min. For positive-ion APPI, ions were generated in an APPI Ion Max source (Thermo Fisher Scientific, Inc., San Jose, CA) operated at a vaporizer temperature of 300 °C. Nitrogen was used as both sheath gas (50 psi) and auxiliary gas (32 mL/min) to minimize oxidation. Gas-phase neutrals were photoionized with a krypton (10 and 10.6 eV photons) ultraviolet lamp (Syagen Technology, Inc., Tustin, CA). Both ionization modes were coupled to a custom-built 21 T FT-ICR mass spectrometer.[55] For each analysis, 1×10^6 charges were accumulated over 1−5 ms in an external multipole ion trap equipped with automatic gain control (AGC). Ions were transferred to the ICR cell based on their m/z ratios using a decreasing auxiliary radio frequency. To maximize the dynamic range and the number of detected peaks, ions were excited to an m/z-dependent radius. Both excitation and detection were performed on the same pair of electrodes in the dynamically harmonized ICR cell, operated with a 6 V trapping potential. Time-domain transients of 3.2 s were acquired using Predator Software, with 100 transients averaged per sample.

Mass Difference Database. A petroleum mass difference database was constructed for the Middle Eastern HVGO sample through meticulous validation of all elemental composition assignments (including heavy isotopes) and evaluation of the resulting error distribution after walking

https://doi.org/10.1021/acs.analchem.5c02420
Anal. Chem. 2025, 97, 18543−18552

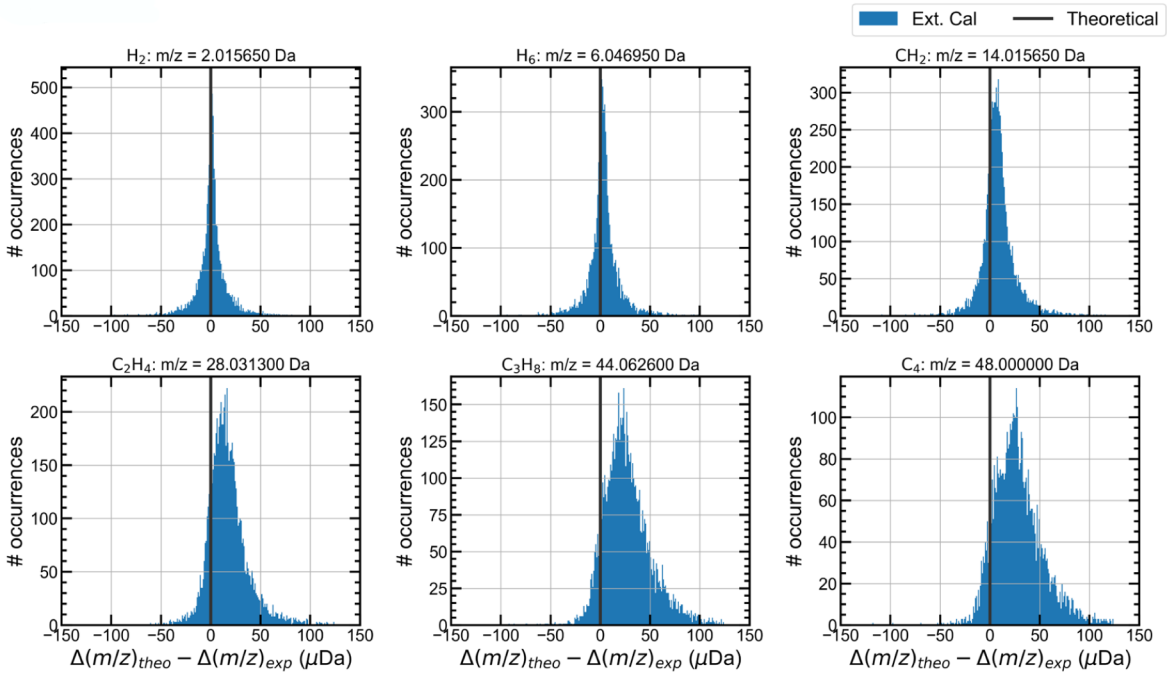

Figure 1. HVGO mass difference distributions derived from the externally calibrated peak list (for $S/N > 6\sigma$) for 6 of the most abundant mass difference distributions that spanned a mass difference between 0 and 50 $\Delta m/z$, at a histogram bin size of 1 μDa. The theoretical mass difference value is denoted by a black, solid vertical line for each distribution, and the x-axis is reported in micro-Dalton.

calibration. The sample was intentionally selected because of its moderate complexity (10,539 peaks > 6σ), known carbon number range (imposed by distillation), and known bulk elemental composition (C, H, N, O, and S). Combined with the mass spectral performance metrics of the 21 T FT-ICR mass spectrometer, we confidently assign 99.89% of the relative abundance in the mass spectrum, the highest percentage known for a petroleum sample to date. In fact, manual assignment of the final remaining unassigned peaks led to the discovery of a series of silicates (identified by mass difference analysis that confirmed the presence of ^{29}Si and ^{30}Si), which had not been previously observed. Figure S1 summarizes the error distribution obtained after walking calibration.

Walking Calibration. A walking calibration was performed after global recalibration as described elsewhere[91] and utilized either carbon number (HVGO) or class (oxygen)/DBE/carbon number series (BO) of a confidently assigned (no other plausible elemental composition within ± 2 ppm), low m/z peak with a $S/N > 10$. Identification and selection of these series will be discussed in detail, later in the manuscript.

Molecular Formula Assignment. Molecular formulas were assigned with PyC2MC[94] using a lowest error algorithm comparing measured m/z values and theoretical values in a molecular formula database. Elemental and isotopic compositions are further refined with constraints on DBE and elemental ratios ($0.2 < H/C < 3$) for both samples, and for the BO sample, ($0 < O/C < 0.8$)). The elemental constraints are defined by sample type and discussed later in the manuscript. The algorithm starts with the peak with the highest S/N and continues in decreasing order. After each monoisotopic formula is assigned, the associated isotopic peaks are assigned before continuing to the next highest S/N peak. Peak lists (uncalibrated, global calibration, mass difference calibrated, and walking calibrated) for both samples highlighted herein (HVGO and bio-oil) are publicly available at Open Science Framework, DOI 10.17605/OSF.IO/D7G3N.

RESULTS AND DISCUSSION

HVGO Mass Difference "Spectrum". A mass difference histogram ("spectrum") was first generated from an externally calibrated mass spectrum by taking the highest m/z peak centroid (m/z_2) and subtracting the value of all lower m/z peak centroids (m/z_1's).[63] The highest m/z value is then removed from the list, and the calculation is repeated until no peaks remain. Note that by design, all mass differences are positive, and the total number of calculations is $[N \times (N\text{-}1)]/2$, where N is the number of peaks. The mass difference histogram (0 − 50 Da) is plotted as the number of occurrences vs mass difference with a bin size of 1 μDa. Figure 1 displays a zoom of the mass difference histogram for six specific intervals that correspond to the masses H_2, H_6, C_1H_2, C_2H_4, C_3H_8, and C_4, which are derived from the externally calibrated HVGO APPI FT-ICR MS peak list. These repeating units, common in petroleum, were selected to span the range $0 < \Delta m < 50$. The theoretical mass differences for these six repeat units are denoted by black, vertical lines. As the mass difference increases (from ~2 to 48 Da), the magnitude of the error between the measured mass differences and the theoretical value increases with a concurrent broadening of the mass difference distribution (from ~10 μDa at H_2 to 50 μDa fwhm at C_4). Neglecting this obvious error and assigning elemental compositions directly from the externally calibrated mass spectrum yields the error distribution shown in Figure 2 (rms error = 280 ppb). To address this issue, we developed a mass difference calibration method, which iteratively adjusts the A and B coefficients in the Ledford equation (eq 1), where m is the mass, z is the charge, and f is the measured cyclotron frequency. This method aligns the mass difference distributions

https://doi.org/10.1021/acs.analchem.5c02420
Anal. Chem. 2025, 97, 18543−18552

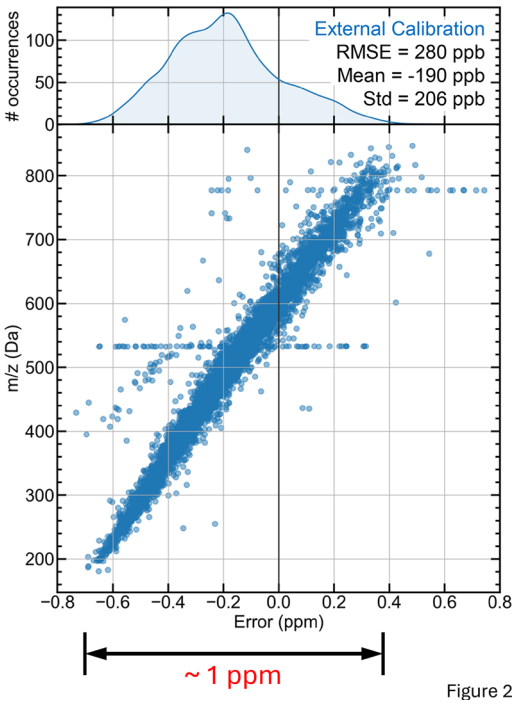

Figure 2

Figure 2. Molecular formula assignment error vs m/z of the externally calibrated HVGO peak list (bottom), and the corresponding error histogram (top). The error range is ∼1.4 ppm, with a mean of −190 ppb, a standard deviation of 206 ppb, and rms error of 280 ppb.

with their theoretical values, as demonstrated in Figure S2, and described below.

$$\frac{m}{z} = \frac{A}{f} + \frac{B}{f^2} \tag{1}$$

HVGO Mass Difference Calibration (MDC). The Ledford equation relates the mass-to-charge ratio (m/z) of an ion to the calibration coefficients A and B, as well as the measured cyclotron frequency. To recalibrate mass differences (Δm), the Ledford equation can be adapted to describe the difference between the m/z values of two peaks i and j (eq 2):

$$\begin{aligned}\Delta(m/z)_{ij} &= \left(\frac{m}{z}\right)_j - \left(\frac{m}{z}\right)_i \\ &= \left(\frac{A}{f_j} + \frac{B}{f_j^2}\right) - \left(\frac{A}{f_i} + \frac{B}{f_i^2}\right) \\ &= A\left(\frac{1}{f_j} - \frac{1}{f_i}\right) + B\left(\frac{1}{f_j^2} - \frac{1}{f_i^2}\right)\end{aligned} \tag{2}$$

The accuracy and precision of the mass difference distributions shown in Figure 1 allow a confident match between the average value of $\Delta(m/z)_{ij}$ and a database of theoretical mass differences Δ_k. The database contains building blocks with $\Delta m/z < 50$ Da, such as C_1, H_1, CH_2, and ^{13}C, among others. A correspondence is thus drawn between measured $\Delta(m/z)_{ij}$ and theoretical Δ_k mass differences.

The calculation of A and B is then an optimization problem in which the following Q least-squares distance between measured and theoretical mass differences is minimized:

$$Q = \sum_k \sum_{(i,j)\in k} \omega_{ij}(\Delta_k - \Delta(m/z)_{ij})^2 \tag{3}$$

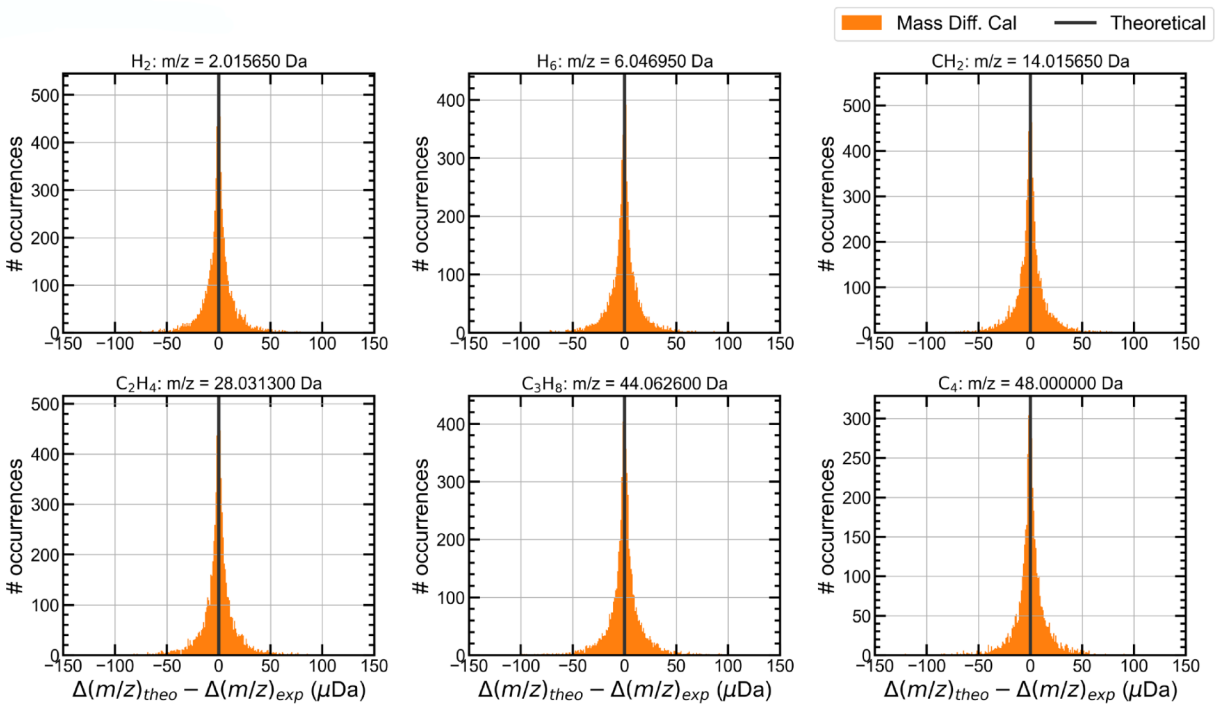

Figure 3. HVGO mass difference distributions after mass difference recalibration (CH_2 distribution, top 25% in S/N) for the same mass differences shown in Figure 1, at a histogram bin size of 1 μDa. The theoretical mass difference value is denoted by a black, solid vertical line for each distribution, and the x-axis is reported in micro-Dalton.

https://doi.org/10.1021/acs.analchem.5c02420
Anal. Chem. 2025, 97, 18543−18552

In the first sum, index k iterates over a set of theoretical m/z differences, noted Δ_k. Then, (i, j) indices iterate over the set of pairs of peaks that correspond to measured m/z differences which contribute to the m/z differences distribution associated to the theoretical m/z difference k. ω_{ij} are weights that can be used to restrain the set of i and j peaks as a function of a third quantity, such as S/N. The selection of peaks based on S/N is discussed below.

For example, considering only one mass difference selected from the mass difference distribution of CH_2 (14.0156501), the equation can be modified to eq 4).

$$A\left(\frac{1}{f_2}-\frac{1}{f_1}\right)+B\left(\frac{1}{f_2^{\,2}}-\frac{1}{f_1^{\,2}}\right)-14.0156501=0 \tag{4}$$

For global calibration, eq 4 can be written for each pair of m/z values belonging to the mass difference distribution of CH_2 (which is depicted in the upper right panel of Figure 1), leading to eq 3. A and B are then iterated such that eq 3 approaches 0. The complete procedure is detailed in Supporting Information and summarized in Figure S2.

Mass difference calibration was performed by selecting $(m/z)_i$ and $(m/z)_j$ pairs based on their average signal-to-noise values. The highest 25% were then used to determine the mass difference distributions and the optimum A and B coefficients. Recalibration of m/z values are computed via the Ledford equation, eq 1), and the optimum A and B coefficients.

Figure 3 reveals the result of the mass difference calibration (MDC) after optimization of the top 25% of the S/N values within the CH_2 mass difference distribution, for the same mass difference pairs shown in Figure 1. The MDC successfully corrected the mass differences to their corresponding theoretical values (black, vertical lines) and narrowed the mass difference distributions. Subsequent molecular formula assignment using the A and B calculated from the top 25% S/N mass difference pairs within the CH_2 mass difference distribution yielded the mass error distribution shown in Figure 4, which can be compared with that obtained from external calibration in Figure S3. The mass difference recalibration successfully recalibrates the mass spectrum without the need for internal calibrants to yield a decreased rms error of 80 ppb. Repeating the same calculation for the 10 most abundant mass difference distributions (individually and collectively) between 0 and 50 Da yielded similar results (Figure S4). Thus, the approach is insensitive to the mass difference distributions selected for recalibration, which highlights the robustness of the method and is achieved because m/z values that comprise each mass difference distribution span a large range of the mass spectrum. The most abundant mass differences and their statical metrics are provided in Table S1.

The effect of S/N filtering (initially top 25%) for subsequent A and B calculation and the resulting impact on molecular formula assignment errors is shown in Figure S5. The weights ω_{ij} in eq 3 are used here to filter mass differences using a criterion on S/N values. As expected, the higher S/N mass pairs yielded the lowest molecular formula assignment errors. Future work will discuss the tradeoff between the use of high S/N mass difference pairs (with higher precision but lower molecular weight range coverage) compared to those with lower S/N threshold values (with lower precision but higher molecular weight range coverage) to calculate optimum A and B coefficients. Walking calibration (discussed later herein) of

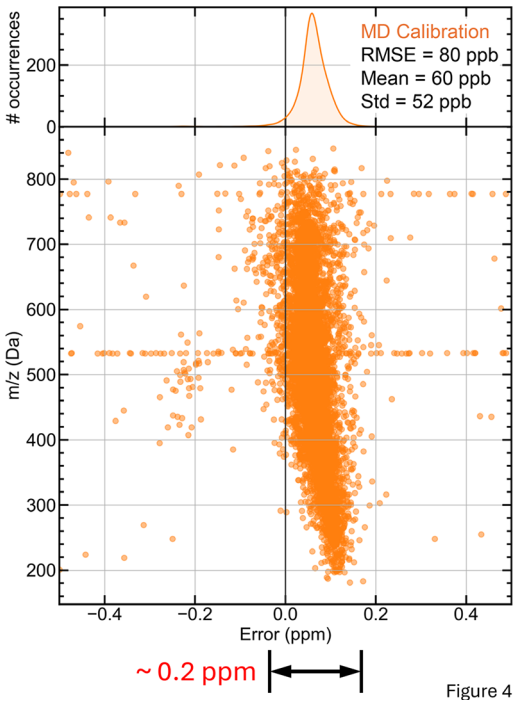

Figure 4

Figure 4. Molecular formula assignment error of the mass difference recalibrated (CH_2 distribution, top 25% in S/N) HVGO peak list (bottom) and corresponding error histogram (top). The error range is ~200 ppb, with a mean of 60 ppb, a standard deviation of 52 ppb, and rms error of 80 ppb.

the mass spectrum yields results similar to those shown in Figure S1.

Bio-Oil Mass Difference Calibration. The peak list from the negative mode ESI analysis of the bio-oil sample (>6σ baseline noise) was subjected to the same mass difference analysis as the HVGO peak list. Adapting the method from one sample to another is straightforward and requires only a choice of the mass difference distributions considered. As we highlighted in the case of the HVGO sample, any of the most abundant mass difference distributions yield similar results. Three of the four most abundant distributions from the mass difference "spectrum" before (blue) and after (orange) mass difference calibration (calculated from the CH_2O mass difference distribution) are displayed in Figure 5. Notably, the displacement of the externally calibrated mass difference distributions for the BO sample (~150 mDa at $\Delta m/z$ of 28 (CO) and 30 (CH_2O)) is markedly greater than that of the HVGO sample at similar $\Delta m/z$ (~20 mDa at $\Delta m/z$ of 28 (C_2H_4)), Figure 1, bottom left). Consequently, forced assignment of the previously determined elemental compositions with the externally calibrated A and B coefficients exposes an abnormally large mass error range (−3.2 to −4.6 ppm) and rms error (3.9 ppm), for external calibration (Figure 6, left, blue). In fact, this particular mass spectrum was selected because of the outdated A and B calibration coefficients and for the nonlinear nature of the error distribution. Thus, it represents one of the "worst case" scenarios for both mass difference and walking recalibration, albeit at high mass resolving power. Mass difference calibration yields a notable improvement (rms error of 354 ppb) in elemental composition mass errors (Figure 6, right, orange). As with the HVGO mass difference calibration, the selection of other abundant mass difference distributions yielded similar recalibration results

https://doi.org/10.1021/acs.analchem.5c02420
Anal. Chem. 2025, 97, 18543−18552

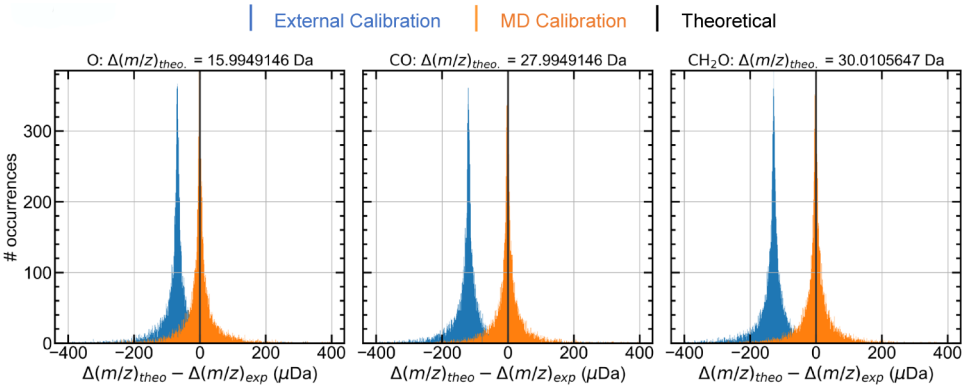

Figure 5. BO mass difference distributions (3 of the 5 most abundant) before (blue) and after (orange) mass difference recalibration (CH_2O distribution, top 25% in S/N), at a histogram bin size of 1 μDa. The theoretical mass difference value is denoted by a black, solid vertical line for each distribution, and the *x*-axis is reported in micro-Dalton.

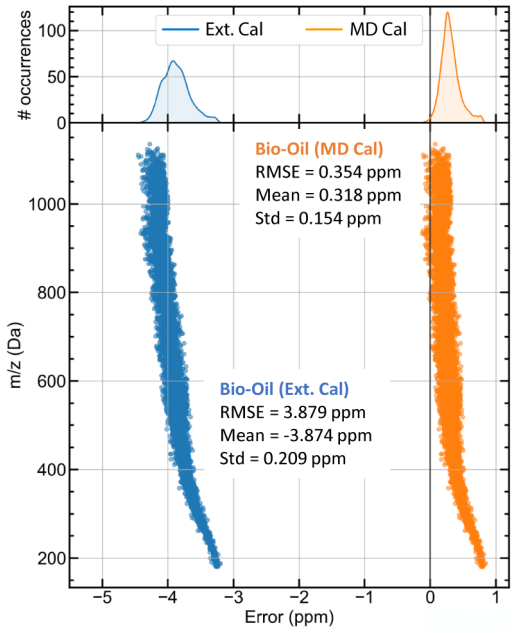

Figure 6. Molecular formula assignment error of the externally calibrated (blue) and mass difference recalibrated (orange) BO peak lists (bottom), and corresponding error histograms (top). After mass difference calibration, the rms error improves to 354 ppb (orange) vs 3879 ppb (blue, external calibration).

(Figure S6), and the impact of S/N filtering on molecular formula assignment errors revealed similar trends for the CH_2O mass difference (Figure S7), which follow the established relationship of increased precision and greater S/N.[95,96] Confirmation that selection of the top 25% S/N mass pairs within any distribution yields those with the highest precision is provided in Figure S8. The abundant O, CO, and CH_2O mass difference histograms before (blue) and after (orange) mass difference calibration are plotted with the top 25% S/N mass pairs in each distribution (top) and all S/N values (bottom), which reveal that the top 25% are clearly the narrower distribution that make up the apex of each of the histograms shown.

Walking Calibration. Although the results presented herein suggest that the mass difference calibration successfully recalibrates externally calibrated mass spectra to yield mass errors of < ± 1 ppm, to test the ability of the approach to correctly identify a confident set of elemental compositions for walking calibration, the method was tested at an allowable mass error of ± 2 ppm. For the HVGO mass difference calibrated peak list, the mass difference "spectrum" ($0 < \Delta m < 50$) was searched to identify which mass difference distributions contained the highest S/N peak. As expected for a petroleum-derived sample, the abundant mass difference distributions were H_2, C_1, C_1H_2, C_2H_4, and C_3H_6, with C_1H_2 being the most abundant. The C_1H_2 mass difference matrix was then filtered to identify a consecutive series that spanned at least 90% of the molecular weight range, under the constraint that it included the highest S/N peak, which resulted in a match.

The lowest m/z member of this 41-member series (m/z = 232.1279983) was then used to calculate plausible elemental compositions with an allowable mass error of ± 2 ppm. Elemental constraints were set to $C_{1-100}H_{2-200}N_{0-4}O_{0-4}S_{0-4}$, with both protonated and radical cations allowed for APPI. The search yielded a single result, $C_{15}H_{20}S_1$, a radical cation with a DBE = 6.5. The proposed elemental composition was verified by intersecting the 41-member calibration matrix, derived from the C_1H_2 mass difference series, with the $^{34}S - {}^{32}S$ mass difference histogram matrix, an approach inspired by the work of Zhang and McElvain.[97] This intersection confirmed the detection of the ^{34}S isotopic peak at its expected theoretical location for the highest S/N members of the calibration series. This step validates both the accuracy of the proposed elemental composition ($C_{15}H_{20}S_1$) and the mass difference calibration method, ensuring that the calibration is chemically and isotopically consistent. Once the elemental composition and calibration matrix were verified, walking calibration was performed as previously described.[91] As the lowest m/z peak in the series was identified, the rest of the series was determined by extending C_1H_2 units across the molecular weight range. This verified series served as a reference point for walking recalibration of the mass spectrum, propagating corrections across nearby peaks. This process ensures improved mass accuracy across the entire molecular weight range of the spectrum.

Walking calibration of the bio-oil sample was performed in a similar manner and relied on the identification of abundant mass difference distributions that contained the highest S/N peak: H_2, C_1, C_1H_2, and O_1. The walking calibration series was constructed from these mass difference matrices by applying recursive criteria, requiring that members of the series form a

https://doi.org/10.1021/acs.analchem.5c02420
Anal. Chem. 2025, 97, 18543−18552

consecutive sequence. This process began with one matrix and involved intersection calculations with the remaining three.

The starting matrix for these calculations (within O mass difference distribution) was determined by which set of successive mass difference pairs included the highest S/N peak in the mass spectrum. Once obtained, the intersection between this series and any of the other mass difference distributions identified the starting points for the repeated identification of successive mass difference series within that mass difference distribution. Once all the consecutive series are identified, an intersection calculation with any of the other 3 distributions starts the process again. The calculation continues until 90% of the molecular weight range ($m/z_{max} - m/z_{min}$) is covered. As the mass differences, or series of mass differences between any 2 peaks in the final matrix is known, the molecular formula assignment of any one of these m/z values results in the confident assignment of all. Thus, to limit the number of possible elemental compositions and molecular formula candidates, the lowest m/z member of the calibration matrix was used (177.0555879). Elemental constraints were set to $C_{1-100}H_{2-200}N_{0-5}O_{0-30}S_{0-5}{}^{10}B_{0-3}{}^{11}B_{0-3}$ with only deprotonated anions allowed ((-) ESI). Possible molecular formulas (five possibilities within ± 2 ppm) include O_3, $O_7{}^{11}B_3$, and $O_3N_1S_1{}^{10}B_3{}^{11}B_1$ classes (less than 1 ppm) and $O_2{}^{10}B_2$/$O_4N_1S_1{}^{10}B_1{}^{11}B_1$ classes (less than 2 ppm). The correct molecular formula (O_3 class) was identified through a final intersection calculation between the walking calibration matrix and the $^{11}B - {}^{10}B$ mass difference matrix, which yielded no matching m/z values (Figure S9). The lack of matches confirms that molecular formulas containing boron isotopes are invalid, leading to the confident assignment of the O_3 class as the correct formula. After the assignment of all molecular formulas within the calibration matrix, a walking calibration is performed. The resulting error distribution is shown in Figure S10.

CONCLUSION

We demonstrate a new global mass calibration and molecular formula assignment algorithm that makes use of the mass differences in a mass spectrum to provide internal calibration without internal calibrants. The mass difference spectrum reveals the presence and absence of particular elements of the periodic table and provides a network of mass differences that are used to confidently assign molecular formulas for walking calibration. Such an approach has obvious applications for mass difference-based walking calibration and the automated elemental composition assignment for all mass spectral peaks in a spectrum. However, it is outside the scope of this manuscript and will be reported in future work. The calibration method is demonstrated here on a petroleum distillate and a bio-oil but has also been applied to other complex matrices (i.e., natural organic matter, perfluoroalkyl substances, and consumer product leachates). We believe the method is general and will find utility in many mass spectrometry applications, especially when control of scan-to-scan ion populations is difficult/impossible (i.e., imaging, LC, and single-particle MS).[80,88,98−100] Finally, we demonstrate the method using 21 T FT-ICR data. In future work, we will apply the method to lower-field ICR data, and to Orbitrap and TOF data for selected applications, which will help to define the lower bound of required resolving power and mass difference accuracy.

ASSOCIATED CONTENT

Supporting Information

The Supporting Information is available free of charge at https://pubs.acs.org/doi/10.1021/acs.analchem.5c02420.

Table S1. Top 12 mass differences from the HVGO APPI mass spectrum after mass difference calibration. The identification and statistical metrics (number of occurrences, theoretical mass difference, mean of the measured mass difference histogram, standard deviation of the measured mass difference histogram to the theoretical value, error in μDa, and ppm error) are provided for each. Figure S1. Molecular formula assignment error of the walking calibrated HVGO peak list. Figure S2. Explanation of the mass difference recalibration procedure. The theoretical mass difference value (CH_2) is denoted by a black, solid vertical line, and the x-axis is reported in micro-Dalton. Figure S3. Molecular formula assignment error of the externally calibrated HVGO (blue) and mass difference recalibrated peak lists (orange), calculated from the CH_2 distribution (top 25% in S/N), along wit the error histograms (right). Figure S4. Molecular formula assignment error (y-axis scale on the left) of the externally calibrated HVGO (blue), mass difference recalibrated (orange) peak lists for each of the top ten mass difference distributions (top 25% in S/N), and for all top ten (top 25% in S/N) mass difference distributions. The number of pairs used in each calculation is shown in gray (y-axis scale on the right). Note, the number of pairs utilized for all ten distributions is given at the top of the column. Figure S5. Molecular formula assignment error (y-axis scale on the left) of the externally calibrated HVGO (blue, far left) and mass difference recalibrated (orange, within the CH_2 distribution) peak lists calculated for each of several different S/N criteria, and for all peaks in the CH_2 mass difference distribution (far right). The number of pairs used in each calculation is shown in gray (y-axis scale on the right). Figure S6. Molecular formula assignment error (y-axis scale on the left) of the externall calibrated BO (blue), mass difference recalibrated (orange) peak lists for each of the top ten mass difference distributions (top 25% in S/N), and for all top ten (top 25% in S/N) mass difference distributions. The number of pairs used in each calculation is shown in gray (y-axis scale on the right). Note, the number of pairs utilized for all ten distributions is given at the top of the column. Figure S7. Molecular formula assignment error (y-axis scale on the left) of the externally calibrated BO (blue, far left) and mass difference recalibrated (orange, within the CH_2 distribution) peak lists calculated for each of several different S/N criteria, and for all peaks in the CH_2 mass difference distribution (far right). The number of pairs used in each calculation is shown in gray (y-axis scale on the right). Figure S8. BO mass difference distributions (3 of the 5 most abundant) before (blue) and after (orange) mass difference recalibration for the CH_2O distribution, top 25% in S/N (top) and all S/Ns (bottom), at a histogram bin size of 1 μDa. The theoretical mass difference value is denoted by a black, solid vertical line for each distribution, and the x-axis is reported in micro-Dalton. Figure S9. BO mass difference

https://doi.org/10.1021/acs.analchem.5c02420
Anal. Chem. 2025, 97, 18543−18552

intersection calculations reveal the absence of abundant overlaps between the O_1 (left) and $^{11}B - {}^{10}B$ (right) mass difference distributions, which eliminates boron-containing species as plausible elemental compositions. The parent distributions for each mass difference are shown in blue, and the intersections between them in orange. Figure S10. Molecular formula assignment error of the walking calibrated BO peak list (PDF)

AUTHOR INFORMATION

Corresponding Authors

Ryan P. Rodgers − *National High Magnetic Field Laboratory, Tallahassee, FL 32310, United States; International Joint Laboratory − iC2MC: Complex Matrices Molecular Characterization, Harfleur 76700, France; Universite de Pau et des Pays de l'Adour, Pau 64000, France; Florida State University, Tallahassee 32306 FL, United States;* orcid.org/0000-0003-1302-2850; Email: rodgers@magnet.fsu.edu

Germain Salvato Vallverdu − *International Joint Laboratory − iC2MC: Complex Matrices Molecular Characterization, Harfleur 76700, France; Universite de Pau et des Pays de l'Adour, Pau 64000, France;* orcid.org/0000-0003-1116-8776; Email: germain.vallverdu@univ-pau.fr

Authors

Christopher L. Hendrickson − *National High Magnetic Field Laboratory, Tallahassee, FL 32310, United States; International Joint Laboratory − iC2MC: Complex Matrices Molecular Characterization, Harfleur 76700, France; Florida State University, Tallahassee 32306 FL, United States;* orcid.org/0000-0002-4272-2939

Christopher A. Holder Montenegro − *Florida State University, Tallahassee 32306 FL, United States*

Alvaro J. Tello-Rodriguez − *Florida State University, Tallahassee 32306 FL, United States*

Teja Potu − *Florida State University, Tallahassee 32306 FL, United States*

Benjohn Shung − *Florida State University, Tallahassee 32306 FL, United States*

Mason Hagan − *Florida State University, Tallahassee 32306 FL, United States*

Chad R. Weisbrod − *National High Magnetic Field Laboratory, Tallahassee, FL 32310, United States;* orcid.org/0000-0001-5324-4525

Pierre Giusti − *International Joint Laboratory − iC2MC: Complex Matrices Molecular Characterization, Harfleur 76700, France; TotalEnergies OneTech, Harfleur 76700, France;* orcid.org/0000-0002-9569-3158

Christopher P. Rüger − *International Joint Laboratory − iC2MC: Complex Matrices Molecular Characterization, Harfleur 76700, France; University of Rostock, Rostock 18055, Germany;* orcid.org/0000-0001-9634-9239

Martha L. Aguilera − *National High Magnetic Field Laboratory, Tallahassee, FL 32310, United States; International Joint Laboratory − iC2MC: Complex Matrices Molecular Characterization, Harfleur 76700, France; Florida State University, Tallahassee 32306 FL, United States;* orcid.org/0000-0002-7273-5343

Complete contact information is available at: https://pubs.acs.org/10.1021/acs.analchem.5c02420

Author Contributions

The manuscript was written through contributions of all authors, and all authors gave approval to the final version of the manuscript.

Notes

The authors declare no competing financial interest.

ACKNOWLEDGMENTS

This work was supported by the National High Magnetic Field Laboratory User Collaboration Grants Program, which is supported by the National Science Foundation Division of Materials Research and Division of Chemistry through DMR-2128556, and the State of Florida. The authors want to thank Donald F. Smith, Amy M. McKenna, Lydia Babcock-Adams, Joseph Frye-Jones (NHMFL), Robert B. Young (CSIRO), Maxime Sueur (TotalEnergies), Carlos Afonso (University of Rouen), and Brice Bouyssiere (Universite de Pau et des Pays de l'Adour) for data contributions and helpful discussions. The authors also thank Helly J. Hansen and Anika Neumann (University of Rostock) for the table of contents figure design.

REFERENCES

(1) Rüger, C. P.; Maillard, J.; Le Maître, J.; Ridgeway, M.; Thompson, C. J.; Schmitz-Afonso, I.; Gautier, T.; Carrasco, N.; Park, M. A.; Giusti, P.; Afonso, C. *J. Am. Soc. Mass Spectrom.* **2019**, *30* (7), 1169.

(2) Somogyi, A.; Oh, C. H.; Smith, M. A.; Lunine, J. I. *J. Am. Soc. Mass Spectrom.* **2005**, *16* (6), 850.

(3) Schmitt-Kopplin, P.; Herir, M.; Kanawati, B.; Tziozis, D.; Hertkorn, N.; Gabelica, Z. *Meteorites* **2012**, *2*, 1−2.

(4) Somogyi, Á.; Thissen, R.; Orthous-Daunay, F. R.; Vuitton, V. *Int. J. Mol. Sci.* **2016**, *17* (4), 439.

(5) Hertzog, J.; Naraoka, H.; Schmitt-Kopplin, P. *Life* **2019**, *9* (2), 48.

(6) Madeira, N. C. L.; Ferreira, P. D. S.; Allochio Filho, J. F.; Chinelatto, L. S.; Cravo, M. C. C.; Martins, A. T.; Lacerda, V.; Romão, W. *Energy Fuels* **2021**, *35* (18), 14553.

(7) Tang, Q.; Zheng, Y.; Liu, T.; Ma, X.; Liao, Y.; Wang, J. *Chem. Eng. J.* **2012**, *207-208*, 2−9.

(8) Neumann, A.; Käfer, U.; Gröger, T.; Wilharm, T.; Zimmermann, R.; Rüger, C. P. *Energy Fuels* **2020**, *34* (9), 10641.

(9) Koolen, H. H. F.; Swarthout, R. F.; Nelson, R. K.; Chen, H.; Krajewski, L. C.; Aeppli, C.; McKenna, A. M.; Rodgers, R. P.; Reddy, C. M. *Energy Fuels* **2015**, *29* (2), 641.

(10) Niles, S. F.; Chacón-Patiño, M. L.; Putnam, S. P.; Rodgers, R. P.; Marshall, A. G. *Environ. Sci. Technol.* **2020**, *54* (14), 8830.

(11) Porto, C. F. C.; Pinto, F. E.; Souza, L. M.; Madeira, N. C. L.; Neto, Á. C.; de Menezes, S. M. C.; Chinelatto, L. S.; Freitas, C. S.; Vaz, B. G.; Lacerda, V.; Romão, W. *Fuel* **2019**, *256*, 115923.

(12) Lacroix-Andrivet, O.; Mendes Siqueira, A. L.; Hubert-Roux, M.; Loutelier-Bourhis, C.; Afonso, C. *Energy Fuels* **2021**, *35* (20), 16432.

(13) Krajewski, L. C.; Rodgers, R. P.; Marshall, A. G. *Anal. Chem.* **2017**, *89* (21), 11318.

(14) Glattke, T. J.; Chacon-Patino, M. L.; Marshall, A. G.; Rodgers, R. P. *Energy Fuels* **2022**, *36* (21), 13060.

(15) D'Andrilli, J.; Dittmar, T.; Koch, B. P.; Purcell, J. M.; Marshall, A. G.; Cooper, W. T. *Rapid Commun. Mass Spectrom.* **2010**, *24* (5), 643.

(16) D'Andrilli, J.; Chanton, J. P.; Glaser, P. H.; Cooper, W. T. *Org. Geochem.* **2010**, *41* (8), 791.

(17) Medeiros, P. M.; Seidel, M.; Ward, N. D.; Carpenter, E. J.; Gomes, H. R.; Niggemann, J.; Krusche, A. V.; Richey, J. E.; Yager, P. L.; Dittmar, T. *Global Biogeochem. Cycles* **2015**, *29* (5), 677.

(18) Dittmar, T.; Koch, B. P. *Mar. Chem.* **2006**, *102* (3−4), 208−217.

(19) Kujawinski, E. B.; Del Vecchio, R.; Blough, N. V.; Klein, G. C.; Marshall, A. G. *In Marine Chem.* **2004**, *92*, 23.
(20) Stubbins, A.; Spencer, R. G. M.; Chen, H.; Hatcher, P. G.; Mopper, K.; Hernes, P. J.; Mwamba, V. L.; Mangangu, A. M.; Wabakanghanzi, J. N.; Six, J. *Limnol. Oceanogr.* **2010**, *55* (4), 1467.
(21) Zhou, Z.; Fu, Q. L.; Fujii, M.; Waite, T. D. *Environ. Sci. Technol.* **2023**, *57* (11), 4690.
(22) Shi, W.; Zhuang, W. E.; Hur, J.; Yang, L. *Water Res.* **2021**, *188*, 116406.
(23) Gaspar, A.; Lucio, M.; Harir, M.; Schmitt-Kopplin, P. *Eur. J. Mass Spectrom.* **2011**, *17* (2), 113−123.
(24) Dong, H.; Cuthbertson, A. A.; Plewa, M. J.; Weisbrod, C. R.; McKenna, A. M.; Richardson, S. D. *Environ. Sci. Technol.* **2023**, *57* (47), 18788.
(25) Richardson, S. D.; Postigo, C. *Comprehen. Anal. Chem.* **2016**, *71*, 335−356.
(26) Luek, J. L.; Schmitt-Kopplin, P.; Mouser, P. J.; Petty, W. T.; Richardson, S. D.; Gonsior, M. *Environ. Sci. Technol.* **2017**, *51* (10), 5377.
(27) Charbonnet, J. A.; McDonough, C. A.; Xiao, F.; Schwichtenberg, T.; Cao, D.; Kaserzon, S.; Thomas, K. V.; Dewapriya, P.; Place, B. J.; Schymanski, E. L.; Field, J. A.; Helbling, D. E.; Higgins, C. P. *Environ. Sci. Technol. Lett.* **2022**, *14*, 473−481.
(28) Bugsel, B.; Zwiener, C. *Anal. Bioanal. Chem.* **2020**, *412* (20), 4797−4805.
(29) Young, R. B.; Pica, N. E.; Sharifan, H.; Chen, H.; Roth, H. K.; Blakney, G. T.; Borch, T.; Higgins, C. P.; Kornuc, J. J.; McKenna, A. M.; Blotevogel, J. *Environ. Sci. Technol.* **2022**, *56* (4), 2455.
(30) Le Maître, J.; Paupy, B.; Hubert-Roux, M.; Marceau, S.; Rüger, C.; Afonso, C.; Giusti, P. *Energy Fuels* **2020**, *34* (8), 9328.
(31) Cho, Y.; Ahmed, A.; Islam, A.; Kim, S. *Mass Spectrom. Rev.* **2015**, *34* (2), 248.
(32) Qian, K.; Robbins, W. K.; Hughey, C. A.; Cooper, H. J.; Rodgers, R. P.; Marshall, A. G. *Energy Fuels* **2001**, *15* (6), 1505.
(33) Marshall, A. G.; Rodgers, R. P. *Acc. Chem. Res.* **2004**, *37* (1), 53.
(34) Franco, D. M. M.; Covas, T. R.; Pereira, R. C. L.; da Silva, L. C.; Rangel, M. D.; Simas, R. C.; Dufrayer, G. H. M.; Vaz, B. G. *Anal. Methods* **2024**, *16* (17), 2635.
(35) Muller, H.; Alawani, N. A.; Naqvi, I. A.; Al-Shammari, M. M.; Al-Bakor, R. Y.; Adam, F. M. *Fuel* **2024**, *358*, 130066.
(36) Griffiths, M. T.; Da Campo, R.; O'Connor, P. B.; Barrow, M. P. *Anal. Chem.* **2014**, *86* (1), 527.
(37) Chen, H.; McKenna, A. M.; Niles, S. F.; Frye, J. W.; Glattke, T. J.; Rodgers, R. P. *Sci. Total Environ.* **2022**, *813*, 151884.
(38) Wise, S. A.; Rodgers, R. P.; Reddy, C. M.; Nelson, R. K.; Kujawinski, E. B.; Wade, T. L.; Campiglia, A. D.; Liu, Z. *Crit. Rev. Anal. Chem.* **2023**, *53*, 1638.
(39) Niles, S. F.; Chacón-Patiño, M. L.; Marshall, A. G.; Rodgers, R. P. *Energy Fuels* **2020**, *34* (11), 14493.
(40) Glattke, T. J.; Chacón-Patiño, M. L.; Marshall, A. G.; Rodgers, R. P. *Energy Fuels* **2020**, *34* (11), 14419.
(41) Shen, M.; Zhu, X.; Shang, H.; Feng, F.; Ok, Y. S.; Zhang, S. *Sci. Total Environ.* **2021**, *756*, 144050.
(42) Chacón-Patiño, M. L.; Mase, C.; Maillard, J. F.; Barrère-Mangote, C.; Dayton, D. C.; Afonso, C.; Giusti, P.; Rodgers, R. P. *Energy Fuels* **2023**, *37* (21), 16612.
(43) Hertzog, J.; Carré, V.; Le Brech, Y.; Dufour, A.; Aubriet, F. *Energy Fuels* **2016**, *30* (7), 5729.
(44) Hertzog, J.; Garnier, C.; Mase, C.; Mariette, S.; Serve, O.; Hubert-Roux, M.; Afonso, C.; Giusti, P.; Barrère-Mangote, C. *J. Anal. Appl. Pyrol.* **2022**, *166*, 105611.
(45) Sudasinghe, N.; Dungan, B.; Lammers, P.; Albrecht, K.; Elliott, D.; Hallen, R.; Schaub, T. *Fuel* **2014**, *119*, 47.
(46) Mase, C.; Moulian, R.; Lazzari, E.; Garnier, C.; Piparo, M.; Hubert-Roux, M.; Afonso, C.; Dayton, D. C.; Barrère-Mangote, C.; Giusti, P. *J. Anal. Appl. Pyrol.* **2024**, *177*, 106354.
(47) Dvorski, S. E. M.; Gonsior, M.; Hertkorn, N.; Uhl, J.; Müller, H.; Griebler, C.; Schmitt-Kopplin, P. *Environ. Sci. Technol.* **2016**, *50* (11), 5536.
(48) Martin, K. R.; Robey, N. M.; Ma, S.; Powers, L. C.; Heyes, A.; Schmitt-Kopplin, P.; Cooper, W. J.; Townsend, T. G.; Gonsior, M. *Environ. Sci.* **2021**, *7* (7), 1250.
(49) Schneider, E.; Giocastro, B.; Rüger, C. P.; Adam, T. W.; Zimmermann, R. *J. Am. Soc. Mass Spectrom.* **2022**, *33* (11), 2019.
(50) Rüger, C. P.; Sklorz, M.; Schwemer, T.; Zimmermann, R. *Anal. Bioanal. Chem.* **2015**, *407* (20), 5923.
(51) Schneider, E.; Czech, H.; Popovicheva, O.; Chichaeva, M.; Kobelev, V.; Kasimov, N.; Minkina, T.; Rüger, C. P.; Zimmermann, R. *Atmos. Chem. Phys.* **2024**, *24* (1), 553.
(52) Ijaz, A.; Kew, W.; Cheng, Z.; Mathai, S.; Lata, N. N.; Kovarik, L.; Schum, S.; China, S.; Mazzoleni, L. R. *Environ. Sci.: Atmos.* **2023**, *3* (10), 1552.
(53) Mazzoleni, L. R.; Saranjampour, P.; Dalbec, M. M.; Samburova, V.; Hallar, A. G.; Zielinska, B.; Lowenthal, D. H.; Kohl, S. *Environ. Chem.* **2012**, *9* (3), 285.
(54) Xie, Q.; Su, S.; Dai, Y.; Hu, W.; Yue, S.; Cao, D.; Jiang, G.; Fu, P. *Environ. Sci. Technol. Lett.* **2022**, *9* (6), 526.
(55) Smith, D. F.; Podgorski, D. C.; Rodgers, R. P.; Blakney, G. T.; Hendrickson, C. L. *Anal. Chem.* **2018**, *90* (3), 2041.
(56) Beu, S. C.; Blakney, G. T.; Quinn, J. P.; Hendrickson, C. L.; Marshall, A. G. *Anal. Chem.* **2004**, *76* (19), 5756.
(57) Kostyukevich, Y. I.; Vladimirov, G. N.; Nikolaev, E. N. *J. Am. Soc. Mass Spectrom.* **2012**, *23* (12), 2198.
(58) Hendrickson, C. L.; Quinn, J. P.; Kaiser, N. K.; Smith, D. F.; Blakney, G. T.; Chen, T.; Marshall, A. G.; Weisbrod, C. R.; Beu, S. C. *J. Am. Soc. Mass Spectrom.* **2015**, *26* (9), 1626.
(59) Bowman, A. P.; Blakney, G. T.; Hendrickson, C. L.; Ellis, S. R.; Heeren, R. M. A.; Smith, D. F. *Anal. Chem.* **2020**, *92* (4), 3133.
(60) Shaw, J. B.; Lin, T. Y.; Leach, F. E.; Tolmachev, A. V.; Tolić, N.; Robinson, E. W.; Koppenaal, D. W.; Paša-Tolić, L. *J. Am. Soc. Mass Spectrom.* **2016**, *27* (12), 1929.
(61) Wootton, C. A.; Maillard, J.; Theisen, A.; Brabeck, G. F.; Schat, C. L.; Rüger, C. P.; Afonso, C.; Giusti, P. *Anal. Chem.* **2024**, *96* (28), 11343−11352.
(62) Kujawinski, E. B.; Behn, M. D. *Anal. Chem.* **2006**, *78* (13), 4363−4373.
(63) Kunenkov, E. V.; Kononikhin, A. S.; Perminova, I. V.; Hertkorn, N.; Gaspar, A.; Schmitt-Kopplin, P.; Popov, I. A.; Garmash, A. V.; Nikolaev, E. N. *Anal. Chem.* **2009**, *81* (24), 10106−10115.
(64) Fouquet, T.; Sato, H. *Mass Spectrom.* **2017**, *6* (1), A0055−A0055.
(65) Gallagher, K. J.; Palasser, M.; Hughes, S.; Mackay, C. L.; Kilgour, D. P. A.; Clarke, D. J. *J. Am. Soc. Mass Spectrom.* **2020**, *31* (3), 700.
(66) Bou-Assaf, G. M.; Chamoun, J. E.; Emmett, M. R.; Fajer, P. G.; Marshall, A. G. *Anal. Chem.* **2010**, *82* (8), 3293.
(67) Rodgers, R. P.; Blumer, E. N.; Emmett, M. R.; Marshall, A. G. *Environ. Sci. Technol.* **2000**, *34* (3), 535.
(68) Snider, R. K. *J. Am. Soc. Mass Spectrom.* **2007**, *18* (8), 1511−1515.
(69) Shi, D.-H.; Hendrickson, C. L.; Marshall, A. G. *Proc. Natl. Acad. Sci.* **1998**, *95* (20), 11532−11537.
(70) Stults, J. T. *Anal. Chem.* **1997**, *69* (10), 1815.
(71) Kind, T.; Fiehn, O. *BMC Bioinf.* **2007**, *8*, 105.
(72) Kendrick, E. *Anal. Chem.* **1963**, *35* (13), 2146−2154.
(73) Biemann, K. *Angewandte Chem.* **1964**, *76* (14), 659.
(74) Tziotis, D.; Hertkorn, N.; Schmitt-Kopplin, P. *Eur. J. Mass Spectrom.* **2011**, *17* (4), 415.
(75) Fouquet, T. N. J. *J. Mass Spectrom.* **2019**, *54* (12), 933−947.
(76) Alton, M. W.; Stark, H. J.; Canagaratna, M. R.; Browne, E. C. *Atmos. Meas. Tech.* **2023**, *16* (12), 3273−3282.
(77) Hughey, C. A.; Hendrickson, C. L.; Rodgers, R. P.; Marshall, A. G.; Qian, K. *Anal. Chem.* **2001**, *73* (19), 4676−4681.
(78) Morgan, T. E.; Ellacott, S. H.; Wootton, C. A.; Barrow, M. P.; Bristow, A. W. T.; Perrier, S.; O'Connor, P. B. *Anal. Chem.* **2018**, *90* (19), 11710.
(79) Merel, S. *Chemosphere* **2023**, *313*, 137443.

https://doi.org/10.1021/acs.analchem.5c02420
Anal. Chem. 2025, 97, 18543−18552

(80) Maillard, J. F.; Demeaux, J.; Mase, C.; Gajan, A.; Tessier, C.; Bernard, P.; Afonso, C.; Giusti, P. *J. Power Sources* **2023**, *582*, 233516.
(81) Traquete, F.; Luz, J.; Cordeiro, C.; Sousa Silva, M.; Ferreira, A. E. N. *Front. Mol. Biosci.* **2022**, *9*, 9.
(82) Yan, B.; Pan, C.; Olman, V. N.; Hettich, R. L.; Xu, Y. Separation of Ion Types in Tandem Mass Spectrometry Data Interpretation-A Graph-Theoretic Approach. *Proceedings. 2004 IEEE Computational Systems Bioinformatics Conference*; IEEE: 2004, pp. 236-244,..
(83) Meija, J. *Anal. Bioanal. Chem.* **2006**, *385*, 486−499.
(84) Forcisi, S.; Moritz, F.; Lucio, M.; Lehmann, R.; Stefan, N.; Schmitt-Kopplin, P. *Anal. Chem.* **2015**, *87* (17), 8917−8924.
(85) Smirnov, K. S.; Forcisi, S.; Moritz, F.; Lucio, M.; Schmitt-Kopplin, P. *Anal. Chem.* **2019**, *91* (5), 3350−3358.
(86) Bruce, J. E.; Anderson, G. A.; Brands, M. D.; Pasa-Tolic, L.; Smith, R. D. *J. Am. Soc. Mass. Spectrom.* **2000**, *11* (5), 416−21.
(87) Wu, S.; Kaiser, N. K.; Meng, D.; Anderson, G. A.; Zhang, K.; Bruce, J. E. *J. Proteome Res.* **2005**, *4* (4), 1434−1441.
(88) Jing, L.; Amster, I. J. *Eur. J. Mass Spectrom.* **2012**, *18* (3), 269−277.
(89) Gavard, R.; Jones, H. E.; Palacio Lozano, D. C.; Thomas, M. J.; Rossell, D.; Spencer, S. E. F.; Barrow, M. P. *Anal. Chem.* **2020**, *92* (5), 3775−3786.
(90) Castilla, C.; Rüger, C. P.; Marcotte, S.; Lavanant, H.; Afonso, C. *J. Am. Soc. Mass Spectrom.* **2020**, *31* (4), 822−831.
(91) Savory, J. J.; Kaiser, N. K.; McKenna, A. M.; Xian, F.; Blakney, G. T.; Rodgers, R. P.; Hendrickson, C. L.; Marshall, A. G. *Anal. Chem.* **2011**, *83* (5), 1732−1736.
(92) Ledford, E. B.; Rempel, D. L.; Gross, M. L. *Anal. Chem.* **1984**, *56* (14), 2744−2748.
(93) Kim, S.; Rodgers, R. P.; Marshall, A. G. *Int. J. Mass Spectrom.* **2006**, *251* (2−3 SPEC. ISS.), 260−265.
(94) Sueur, M.; Maillard, J. F.; Lacroix-Andrivet, O.; Rüger, C. P.; Giusti, P.; Lavanant, H.; Afonso, C. *J. Am. Soc. Mass Spectrom.* **2023**, *34* (4), 617.
(95) Marshall, A. G. *Anal. Chem.* **1979**, *51* (11), 1710−1714.
(96) Chen, L.; Cottrell, C. E.; Marshall, A. G. *Chemom. Intell. Lab. Syst.* **1986**, *1*, 51−58.
(97) Zhang, Z.; McElvain, J. S. *Anal. Chem.* **2000**, *72* (11), 2337−2350.
(98) Ellis, S. R.; Bruinen, A. L.; Heeren, R. M. A. *In Anal. Bioanal. Chem.* **2014**, *406*, 1275.
(99) Smith, D. F.; Kharchenko, A.; Konijnenburg, M.; Klinkert, I.; Paša-Tolić, L.; Heeren, R. M. A. *J. Am. Soc. Mass Spectrom.* **2012**, *23* (11), 1865.
(100) Zhu, S.; Li, L.; Wang, S.; Li, M.; Liu, Y.; Lu, X.; Chen, H.; Wang, L.; Chen, J.; Zhou, Z.; Yang, X.; Wang, X. *Atmos. Meas. Tech.* **2020**, *13* (8), 4111.

https://doi.org/10.1021/acs.analchem.5c02420
Anal. Chem. 2025, 97, 18543−18552